Kinoform using an electrically controlled birefringent liquid-crystal spatial light modulator

Jun Amako and Tomio Sonehara

A programmable kinoform using an electrically controlled birefringent liquid-crystal spatial modulator (ECB-LCSLM) is discussed. The LCSLM is capable of continuous phase modulation from 0 to 2π. For the kinoform generation, the phase distribution is calculated by iterative methods and recorded on the LCSLM with 16 quantizing levels. We discuss the characteristics and the structure of the LCSLM for the implementation of the programmable kinoform while comparing the computed results and optical reconstructions.

Key words: Kinoform, spatial light modulator, liquid crystal, thin-film transistor active matrix, electrically controlled birefringent mode, phase shift.

Introduction

A programmable hologram is an attractive and useful device in many applications including laser beam steering, optical computing, and three-dimensional motion pictures. One of the ways of making a hologram is to record it on a spatial light modulator by a computer-synthesized method. Specifically, the liquid-crystal spatial light modulator (LCSLM) is suitable because of operation at low voltage, low power consumption, matrix-addressing capability, and flexibility of design. Recently there have been reports on the programmable computer-generated hologram (CGH)[1–3] when commercially available twisted-nematic, liquid-crystal (TN-LC) display devices were used. Since both amplitude and phase modulation occur simultaneously in the TN mode, the TN-LC devices are not applicable for a phase-only modulator. To obtain phase-only modulation, the applied voltage must be kept in the range of constant amplitude modulation, which is limited below the threshold voltage of the amplitude modulation.[4] Because the phase modulation depth is limited to under 2π, the conventional phase-type CGH requires binary quantization of 0 to π stable states with equal magnitude of amplitude.[1,2] The CGH has high quantization noise. On the other hand, when recording an amplitude-type CGH, low light efficiency remains a problem, although quantization noise can be reduced by using a good linearity of transmittance to the applied voltage.[3]

The objective of this research is to examine the feasibility of a programmable kinoform[5] by using a LCSLM. To record the kinoform, we designed the ECB (electrically controlled birefringent)-LCSLM, which is characterized by a homogeneous LC layer in which the molecular alignment on the input and output face is parallel and different from the 90° alignment of the TN mode. This alignment enabled us to utilize the maximum change of birefringence when the polarizaiton of the incident light is parallel to the LC directors. Therefore, our LCSLM has phase modulation from 0 to 2π, keeping the magnitude of amplitude constant.

To drive the LCSLM, we employed a thin-film transistor (TFT) active matrix method that has the advantages of low cross talk and linear phase modulation to the applied voltage. By using iterative methods,[6,7] we calculated the phase distribution of the pixel in the TFT-LCSLM.

For high-quality reconstruction, we discuss the following points: how to calculate and record the kinoform, how to optimize the phase modulation characteristics of the LCSLM, and how to modify the structure of the LCSLM.

Liquid-Crystal Spatial Light Modulator

Recording the kinoform requires a continuous phase modulation between 0 and 2π and a constant amplitude. We employed an ECB-LCSLM.

When fabricating the ECB-LCSLM, the material, molecular alignment, and thickness of the LC layer

The authors are with the R&D Division, Seiko Epson Corporation, Owa 3-3-5, Suwa-shi, Nagano 392, Japan.

Received 12 October 1990.
0003-6935/91/324622-07$05.00/0.

are important factors. These factors should be chosen by taking the following points into consideration:

(1) Phase modulation over 2π and linearity of phase shift to applied voltage. Nonlinearity increases the quantization noise in the reconstructed image.

(2) No amplitude modulation during the full range of the phase modulation. Amplitude modulation causes degradation in the quality of the reconstructed image.

(3) Thin LC layer. The response of the LCSLM becomes slow in proportion to the square of the LC layer thickness. Slow response limits the versatility of the LCSLM as a programmable optical device.

The LCSLM we fabricated has a homogeneous LC layer in which the LC molecules at the off state were aligned parallel with the panel faces. The retardation is set to 1.25 μm at 632.8-nm wavelength, where the birefringence at the off state was 0.209 and the thickness of the LC layer was 6.0 μm. In a display area of 25.6 × 19.8 mm, there are 320 × 220 pixels, and the pixel size is 80 × 90 μm. Our LCSLM is an active matrix type and has a polycrystalline Si TFT circuit in each pixel. Our polycrystalline Si TFT driving method has been developed for LC television[8] and projection displays.[9] An active matrix LCSLM displays lower cross talk and better linearity of electro-optic response to the applied voltage than a simple multiplexed-type LC display device. The overview of the LCSLM and its pixel structure is shown in Figs. 1(a) and 1(b), respectively. The operating principle of the LCSLM has been described elsewhere[8] and is not covered here.

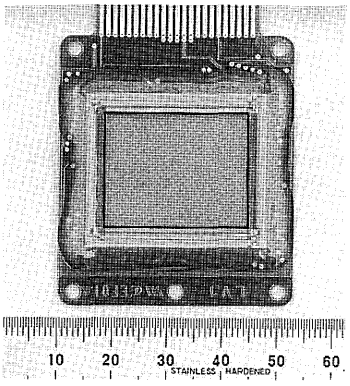

(a)

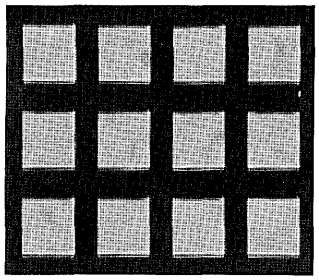

(b)

Fig. 1. (a) Overview of the LCSLM, (b) its pixel structure.

Light Modulation Characteristics

First, we measured the light modulation characteristics of the LCSLM. The experimental results are shown in Fig. 2, where the phase shift and intensity transmittance are plotted as a function of applied voltage. In all the experiments, a linearly polarized He–Ne laser (632.8 nm) was used as the light source. The collimated laser beam enters the device that is located between a pair of parallel polarizers. The transmission axes of these polarizers are set in parallel with the LC directors. Higher diffraction orders due to the regular pixel structure of the device were filtered out by using a long-focal-length lens and a slit. A Mach–Zehnder interferometer was used to measure the dependence of the phase modulation on applied voltage. The applied voltage in the following figures was measured at the external terminal on the peripheral circuit of the LCSLM.

As shown in Fig. 2, we can obtain more than 2π continuous phase modulation and good linearity between 2.0 and 3.5 V. However, an unexpected ±10% modulation of the transmittance is observed. This is caused by imperfect alignment of the LC molecules on the TFT substrate, on which the transistors appear as projections on the surface of the substrate.

While the ±10% modulation of the transmittance still remains, our ECB-LCSLM can produce high-performance kinoforms as described in the next section.

Next, we record a phase grating on the LCSLM as a parameter of quantization to confirm the blazed effect featured by kinforms. The distribution of the phase for a grating period and the intensity profile of a Fraunhofer diffraction pattern with quantizing levels of 2, 4, 8, and 16 are shown in Figs. 3(a)–3(d), respectively. One grating period consists of 16 data lines of the LCSLM. The intensity profile was de-

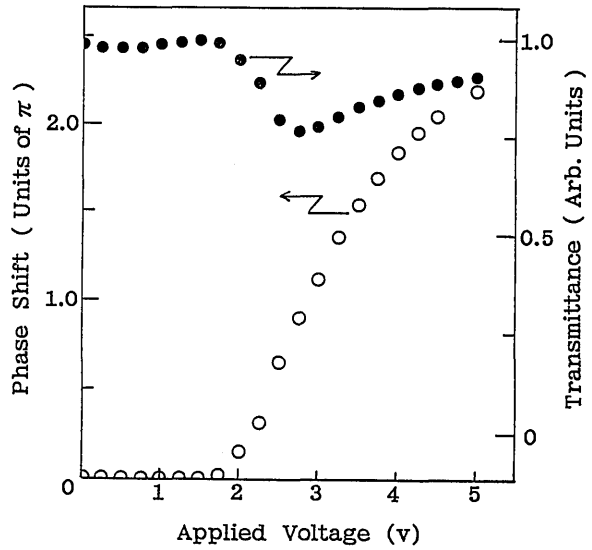

Fig. 2. Phase shift and transmittance versus applied voltage: ○ phase shift; ●, transmittance. The LCSLM was in the ECB mode with the off-state molecular orientation aligned parallel to the panel faces.

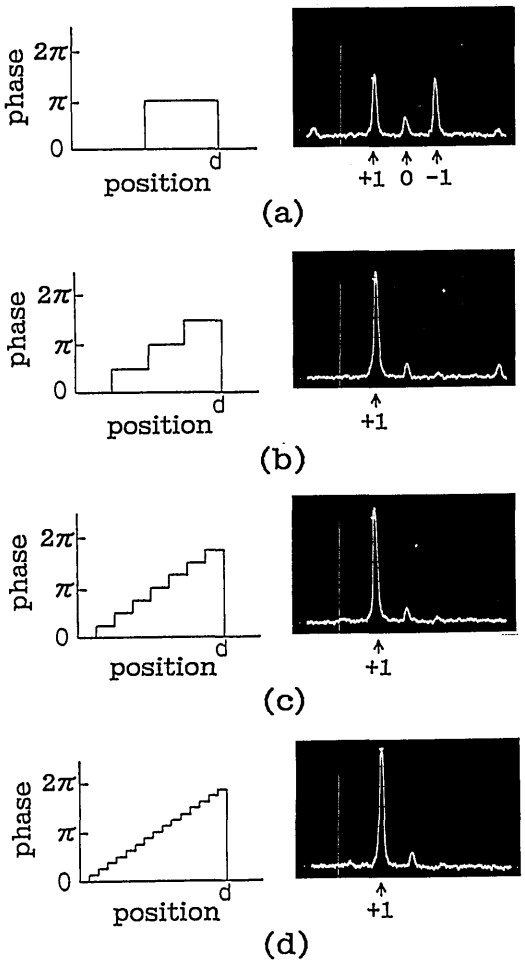

Fig. 3. Phase distribution and Fraunhofer diffraction pattern of the grating recorded on the LCSLM. The quantizing levels are (a) 2, (b) 4, (c) 8, and (d) 16. One grating period is marked with the letter d. Dead regions between the pixels are omitted in the drawings of the phase functions.

tected by a video camera. Two peaks of ±1 diffraction appear with the same strength in Fig. 3(a). This is always observed for a binary phase grating. On the other hand, the peak of +1 order in Figs. 3(b)–3(d) becomes stronger with an increase of quantizing levels, while other peaks are well suppressed. The residual energy of the zero order, which should theoretically be zero, is probably due to a combination of some of the following effects: nonlinearity at relatively high voltage regions as seen in Fig. 2, nonuniformity of phase modulation among pixels, and insufficient resolution of 12 lines/mm.

To support the experiments, some theoretical discussion is required. For the multilevel phase grating, mth-order diffraction efficiency η_m can be expressed by

$$\eta_m = \mathrm{sinc}^2(\pi m/Q)\left|\sum_{k=1}^{Q}\exp[i(\phi - 2\pi m)k/Q]/Q\right|^2, \quad (1)$$

where Q is the number of quantizing levels and ϕ is the phase difference between the top and the bottom of the grating. Equation (1) is derived from the Fourier transform of the phase distribution of the grating. When the phase-matching condition is met, that is, $\phi = 2\pi$, the efficiencies η_{+1} of the +1 order for $Q = 2$, 4, 8, and 16 are obtained as 0.41, 0.81, 0.95, and 0.99, respectively, while the efficiency η_0 of 0 order is 0 for any values of Q, and the efficiency η_{-1} of the −1 order is 0.41 for $Q = 2$ or 0 for others. In general, however, some effects as described earlier introduce phase mismatching ($\phi \neq 2\pi$). Therefore η_{+1} is decreased while both η_0 and η_{-1} are increased, which means residual energy exists for 0 and +1 orders.

From these results and analyses, we confirm that our system can properly supply the signal to the LCSLM, and as a result of this, the LCSLM can function as a high-efficiency phase grating.

Writing and Reading a Kinoform

We describe the method of recording the kinoform on the LCSLM and the results of its reconstruction.

We calculate the phase distribution of the kinoform by using iterative methods.[6,7] These methods enable us to reduce quantization errors by taking into account the display performance of a device (the LCSLM in our case) and iteratively optimizing the kinoform. The principal steps of the calculation proceed as follows.

The kth trial solution for the input image $g_k(\mathbf{x})$ is Fourier transformed, yielding

$$G_k(\mathbf{u}) = |G_k(\mathbf{u})|\exp[i\phi_k(\mathbf{u})], \quad (2)$$

where the vector $\mathbf{x}$ may be a spatial coordinate, and the vector $\mathbf{u}$ may be a spatial frequency coordinate. $G_k(\mathbf{u})$ is then made to fulfill the constraints in the Fourier domain. These constraints are that the Fourier transform has the constant amplitude of A_k and the multilevel quantized phase of $\tilde{\phi}_k(u)$. We note that A_k should be the average of $|G_k(\mathbf{u})|$ and the number of phase levels should be determined considering the signal resolution supported by the LCSLM and its driving unit. In this way the modified transform $G_k'(\mathbf{u})$ is given by

$$G_k'(\mathbf{u}) = A_k\exp[i\tilde{\phi}_k(\mathbf{u})]. \quad (3)$$

$G_k'(u)$ is inverse Fourier transformed yielding the complex amplitude of the reconstructed image $g_k'(\mathbf{x})$. Then the kth iteration is completed by forming a new trial $g_{k+1}(\mathbf{x})$ for the next iteration by making $g_k'(\mathbf{x})$ fulfill the constraints in the object domain. The first iteration is started by multiplying an input image $f(\mathbf{x})$ with random phase. The iterations continue until the error in the reconstructed image is reduced and approaches a limit.

By using computer simulations, we tested the ability of two approaches: the error-reduction approach[6] and the input–output approach.[7] We used the constraints in the object domain that are defined in

the error-reduction approach by

$$g_{k+1} = |f(\mathbf{x})|\, g_k'(\mathbf{x}) / |g_k'(\mathbf{x})|, \quad (4)$$

and in the input–output approach by

$$g_{k+1} = g_k(\mathbf{x}) + \beta[\,|f(\mathbf{x})|\, g_k'(\mathbf{x}) / |g_k'(\mathbf{x})| - g_k'(\mathbf{x})] + \beta[\,|f(\mathbf{x})|\, g_k'(\mathbf{x}) / |g_k'(\mathbf{x})| - |f(\mathbf{x})|\, g_k(\mathbf{x}) / |g_k(\mathbf{x})|]. \quad (5)$$

In Eq. (5), β is the dumping factor. We set β to 1.0 in our simulations described below.

In a series of calculations, parameters are the number of quantizing levels, the number of sampling points, and the design of input binary images. We verified that the input–output approach results in faster uniformity with less quantization error than the error-reduction approach as pointed out by Fienup.[7] For this reason we decided to employ the input–output approach in our experiments.

After the phase distribution of the kinoform is computed, the corresponding video signal is provided by a personal computer. The signal was supplied to the LCSLM through buffer memories. Quantization of the signal is limited to up to 16 by the analog-to-digital conversion board (4-bit resolution) used in our experimental system. Fast rewriting of the kinoform becomes possible by reading preloaded pattern information from the video memories of the personal computer.

By using the experimental system, reconstruction of the kinoform is implemented. The first example is for a binary (= 0 or 1) image (a bird). The image was sampled on a 128 × 128 grid to compute the kinoform. The image intensity is represented by one (one bit) for the white part of the sampled area or by zero (zero bit) for the black part. Figure 4 shows the range of computed image intensities as a function of the number of iterations. Here, the results for different quantizing levels are compared. For the quantization of 2 levels, the iterative process could barely reduce quantization error. For 16 levels, the error can be substantially reduced after a few iterations and shows little change after 10–20 iterations. According to these results, the phase distribution after 50 iterations can be recorded on the LCSLM by using a 128 × 128 pixel field in each case. The optical reconstructions of these kinoforms are shown in Fig. 5. When the kinoform is quantized into two levels [Fig. 5(a)], double images and large nonuniformity of the intensity are clearly seen as in Fig. 5(b). This is why a binary kinoform is not used in practical applications. When the kinoform is quantized into 16 levels [Fig. 5(c)], improvement is noticed. As a consequence, the energy dissipation to the conjugate image is well suppressed and only the desired image can be brightly reconstructed as shown in Fig. 5(d). The phase distributions shown in the figures are displayed with 16 gray levels.

The second example is the binary image of an array of spots. The image was sampled on a 128 × 128 grid. Figure 6 shows the range of the computed image intensity as a function of the number of iterations. The image was a line of 1 × 13 spots. The optimized phase distribution after 50 iterations was recorded on the LCSLM when a 128 × 128 pixel field was used. The 1 × 13 spots were optically reconstructed and their intensity profiles are shown in Figs. 7(a) and 7(b), respectively. Figure 8 is the range of computed image intensities for an array of 13 × 13 spots. The kinoform was recorded on the LCSLM in a way that is similar to that in Fig. 7. The 13 × 13 spots were optically reconstructed and their intensity profiles are shown in Figs. 9(a) and 9(b), respectively, where

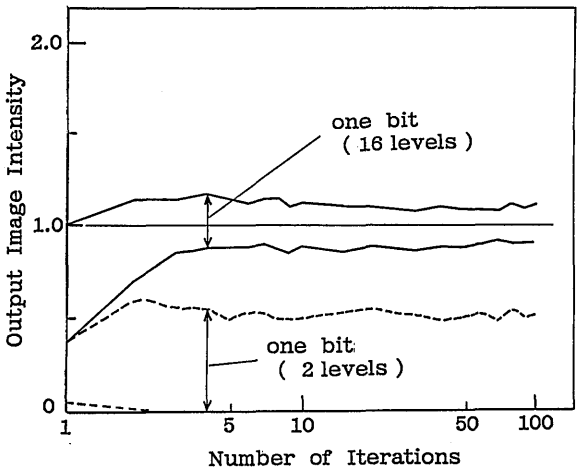

Fig. 4. Range of the computed image intensity versus the number of iterations. A binary image (a bird) was sampled on a 128 × 128 grid: dashed curves, 2 quantizing levels; solid curves, 16 quantizing levels.

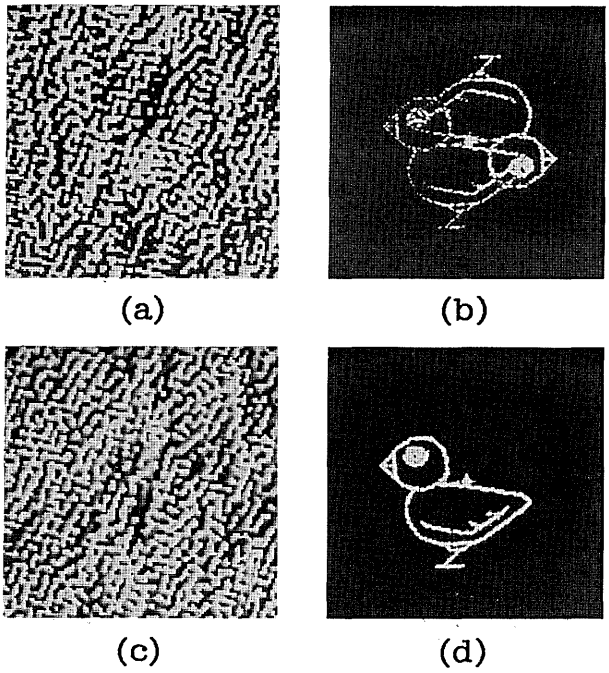

Fig. 5. (a), (c) Kinoform of the binary image (a bird); (b), (d) its optical reconstruction. A 128 × 128 pixel field was used to record the kinoform on the LCSLM. The quantizing levels were (a), (b) 2 and (c), (d) 16.

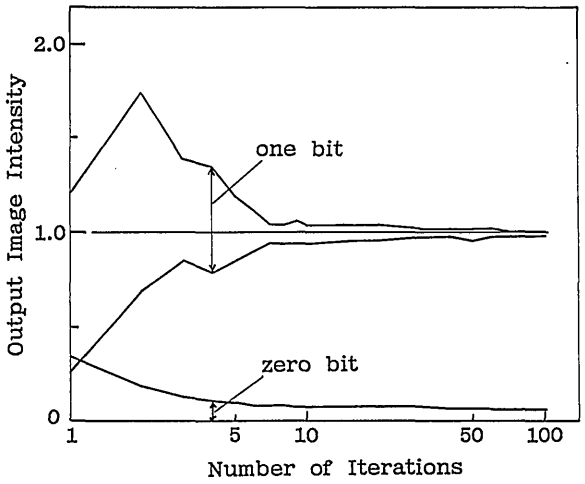

Fig. 6. Range of the computed image intensity versus the number of iterations. A binary image of 1 × 13 spots was sampled on a 128 × 128 grid. The number of quantizing levels was 16.

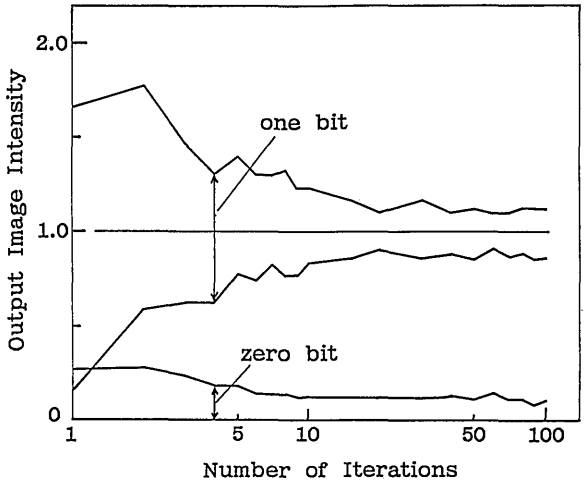

Fig. 8. Range of the computed image intensity versus the number of iterations. A binary image of 13 × 13 spots was used. The other conditions are the same as those in Fig. 6.

the peak of the zero order was deliberately suppressed to observe details of the spots. As seen in the figures, the energy of the incident light is well focused on the desired points of the output plane. Considering the good agreement between the deviation of the computed intensity and that of the optical reconstruction, the nonuniformity of the spots can be mainly due to the lack of quantizing levels rather than the nonlinearity and the nonuniformity of the phase modulation characteristics.

The generation of an array of spots as described above can be used for an array illumination in optical data processing. An array illuminator efficiently converts a wide beam into an array of bright spots. These spots are to be used to illuminate the array of microdevices in an optical computer.

Discussion

As mentioned in the previous sections, the kinoform recorded on our LCSLM exhibits successful reconstructions. However, a few problems remain to be solved. These problems could be solved as follows:

The first solution is to optimize the LC molecular alignment and the retardation of the LC layer. This would improve the linearity of phase modulation to applied voltage. Another solution would be to compensate for nonuniformity of the phase modulation characteristics among pixels. This can be achieved by

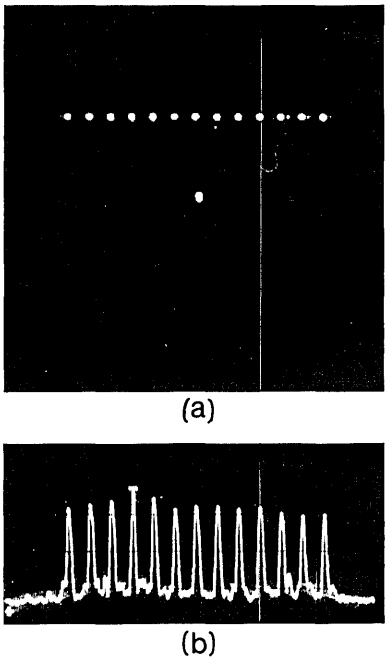

Fig. 7. (a) Reconstructed image of 1 × 13 spots, (b) the intensity profile in the output plane. A 128 × 128 pixel field was used to record the kinoform.

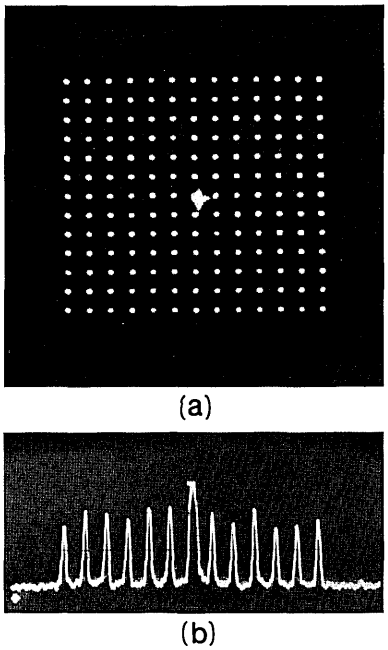

Fig. 9. (a) Reconstructed image of 13 × 13 spots, (b) the intensity profile in the output plane (including the spot of the zero order). The other conditions are the same as in Fig. 7.

DOCKET ALARM

Explore Litigation Insights

Docket Alarm provides insights to develop a more informed litigation strategy and the peace of mind of knowing you're on top of things.

Real-Time Litigation Alerts

Keep your litigation team up-to-date with **real-time alerts** and advanced team management tools built for the enterprise, all while greatly reducing PACER spend.

Our comprehensive service means we can handle Federal, State, and Administrative courts across the country.

Advanced Docket Research

With over 230 million records, Docket Alarm's cloud-native docket research platform finds what other services can't. Coverage includes Federal, State, plus PTAB, TTAB, ITC and NLRB decisions, all in one place.

Identify arguments that have been successful in the past with full text, pinpoint searching. Link to case law cited within any court document via Fastcase.

Analytics At Your Fingertips

Learn what happened the last time a particular judge, opposing counsel or company faced cases similar to yours.

Advanced out-of-the-box PTAB and TTAB analytics are always at your fingertips.

API

Docket Alarm offers a powerful API (application programming interface) to developers that want to integrate case filings into their apps.

LAW FIRMS
Build custom dashboards for your attorneys and clients with live data direct from the court.

Automate many repetitive legal tasks like conflict checks, document management, and marketing.

FINANCIAL INSTITUTIONS
Litigation and bankruptcy checks for companies and debtors.

E-DISCOVERY AND LEGAL VENDORS
Sync your system to PACER to automate legal marketing.